Nat. Hazards Earth Syst. Sci. Discuss., https://doi.org/10.5194/nhess-2017-310
Manuscript under review for journal Nat. Hazards Earth Syst. Sci.
Discussion started: 16 January 2018

Natural Hazards and Earth System Sciences
Discussions

Identifying a Transition Climate Zone in an Arid River Basin using a Hydrological Drought Index

Libo Zhang[1], Yongqiang Liu[2], Lu Hao[1], Decheng Zhou[1], Cen Pan[1], Peilong Liu[1], Zhe Xiong[3], Ge Sun[4]

[1]Jiangsu Key Laboratory of Agricultural Meteorology, International Center for Meteorology, Ecology, and Environment, College of Applied Meteorology, Nanjing University of Information Science and Technology, Nanjing, China
[2]Center for Forest Disturbance Science, USDA Forest Service, Athens, Georgia, USA
[3]Institute of Atmospheric Physics, Chinese Academy of Sciences, Beijing, China
[4]Eastern Forest Environmental Threat Assessment Center, USDA Forest Service, Raleigh, North Carolina, USA

Correspondence to: Yongqiang Liu (yliu@fs.fed.us)

Abstract. Drought indices have been widely used in climate classification. However, there is not enough evidence for their ability in identifying the multiple climate types in areas with complex topography and landscape, especially in those areas with a transition climate. This study compares a meteorological drought index, the aridity index (*AI*) defined as the ratio of precipitation (*P*) to potential evapotranspiration (*PET*), with a hydrological drought index, the evaporative stress index (*ESI*) defined as the ratio of actual evapotranspiration (*AET*) to *PET*. We conducted this study using modeled high resolution climate data for period of 1980-2010 in the Heihe River Basin (HRB) in the arid northwestern China. *PET* was estimated using the Penman-Monteith and Hamon methods. The climate classified by *AI* shows two distinct climate types for the upper and the middle and lower basin reaches, while three types were found if *ESI* was used. This difference indicates that only *ESI* is able to identify a transition climate zone in the middle basin. This contrast between the two indices is also seen in the inter-annual variability and extreme dry / wet events. The magnitude of variability in the middle basin is close to that in the lower basin for *AI*, but different for *ESI*. *AI* has larger magnitude of the relative inter-annual variability and greater decreasing rate from 1980-2010 than *ESI*, suggesting the role of local hydrological processes in moderating extreme climate events. Thus, the hydrological drought index is better than the meteorological drought index for climate classification in the arid Heihe River Basin where local climate is largely determined by topography and landscape. We

Nat. Hazards Earth Syst. Sci. Discuss., https://doi.org/10.5194/nhess-2017-310
Manuscript under review for journal Nat. Hazards Earth Syst. Sci.
Discussion started: 16 January 2018

conclude that the land-surface processes and human disturbances play an important role in altering hydrological drought conditions and their spatial and temporal variability.

1 Introduction

Large river basins at continental and sub-continental scales usually encompass multiple climate types related to complex topography and landscape. Climate is more humid in the upper basin near the river origins with high elevations and forest and / or permanent snow cover than the lower basin with low elevations and less vegetated lands. Climate could be extremely dry in parts of a watershed under a prevailing atmospheric high pressure system. The sub-continental Colorado River watershed, for example, is dominated by cold and humid continental climate in the upper basin of the Rocky Mountains and cold semi-arid or warm desert climate in the lower basin of the southern inter-mountains.

This feature of multiple climate types is also seen in some smaller basins. The Heihe River Basin (HRB) in northwestern China, for example, has an area of 130, 000 km^2 with annual precipitation varying dramatically from about 500 mm in the upper basin of the Qilian Mountains with forest-meadow-ice covers in the south to less than 100 mm in the lower basin of the Alxa High Plain with Gobi and sandy lands in the north. Climate types change from cold and humid continental to arid desert, accordingly.

The relative high precipitation in the humid upper basin supports forests and meadows and provides source water lower reaches of the Heihe River. In contrast, water is a major limitation factor in arid lower basin. In addition, more extreme weather conditions, especially droughts, occur in arid lower basin. In the Colorado River basins, the reconstructed data show decadal periods of persistently low flows during the past centuries (Woodhouse et al., 2010). The drought severity in the new millennia has been the most extreme over a century (Cayan et al., 2010). The reconstructed precipitation series in the HRB indicates that droughts were much more frequent and lasted longer than floods in the past two centuries (Ren et al., 2010). Droughts occurred more often in the dry lower basin than the humid upper basin (Li, 2012).

The watersheds with varied topography and landscape may have a transition climate zone between the two zones. In the HRB, for example, the Koppen climate classification (Peel et al., 2007) shows polar tundra or boreal climate in the upper basin of the mountain regions in the south, arid desert climate in the lower basin in the north, and a transition zone of steppe climate

Nat. Hazards Earth Syst. Sci. Discuss., https://doi.org/10.5194/nhess-2017-310
Manuscript under review for journal Nat. Hazards Earth Syst. Sci.
Discussion started: 16 January 2018

in the middle. Identifying this transition zone and understanding its unique climate features are of both scientific and management significance. The complex topography in upper basin and harsh climate in lower basin make both regions unsuitable for human living. The transition zone however is relatively flat in comparison with the mountain region and less arid in comparison with the dryland region. It therefore provides a favorable condition for industrial and agricultural development. Also, the environmental conditions in this region are more dynamical and localized because of human induced rapid and fragmental landscape changes.

The Koppen climate classification, one of the most widely used climate classification techniques at large geographic scales and constructed based on the properties of ecosystems, latitude, and average and seasonal precipitation and temperature, is often used for a large region with static environmental conditions. Drought indices are another useful tool to classify and monitor aridity and drought of a region. Drought indices are mainly determined by precipitation, and the ground surface temperature and evapotranspiration, all of which are strongly affected by local landscape and topography. The aridity index (AI) (Budyko, 1974) is one of the widely used drought indices (UNESCO, 1979; Wolfe, 1997; Onder, 2009). It is also used as an essential element in many other indices to describe actual drought conditions (Arora, 2002). The AI defines the dryness degree based on the relative magnitude of water demand and supply and calculated based on average precipitation and potential evapotranspiration, which is in turn determined by temperature. The AI therefore is a meteorological drought index.

Hydrological drought indices such as evaporative stress index (ESI) are also widely used in climate and hydrological studies. This type of indices is determined not only by meteorological conditions but also the surface hydrological properties and processes such as soil moisture, groundwater, and evapotranspiration etc. The ESI defines the dryness degree of a region based on the ratio of actual (AET) to potential evapotranspiration (PET). A relatively low ESI indicates water limitation to plants and the actual rate is way below the PET. In contrast, a relatively high ESI indicates freely available water with the AET rate approaching or close to the PET. The ESI has been long used to evaluate the irrigation need for crop growth and land classification (Yao 1974). The ESI has been used recently to evaluate water stress using remotely sensed hydrological and ecological properties (Anderson et al., 2016).

Nat. Hazards Earth Syst. Sci. Discuss., https://doi.org/10.5194/nhess-2017-310
Manuscript under review for journal Nat. Hazards Earth Syst. Sci.
Discussion started: 16 January 2018

Many studies have compared various types of drought indices in different climatic environments. Otkin et al. (2013) compared the ESI with drought classification used by the U.S. Drought Monitor (USDM) (Svoboda et al., 2002) and found that the ESI anomalies led the USDM drought depiction by several weeks and large ESI anomalies therefore were indicative of rapidly drying conditions. This finding was coincident with the droughts occurred across the United States in recent years. Choi et al. (2013) compared the ESI with the Palmer drought severity index (PDSI) in a watershed of the Savannah River branch in southeastern United States during 2000-2008. They found that the ability of the ESI to capture shorter term droughts was equal or superior to the PDSI when characterizing droughts for the watershed with a relatively flat topography dominated by a single land cover type. However, the differences between the meteorological and hydrological drought indices in capturing the spatial patterns and temporal variations under complex topography and environments, especially with a transition zone, are not well characterized and understood.

This study is to understand the two different drought indices of AI and ESI in their capacity in identifying the transition climate zone in the HRB. It was made mainly by comparing the spatial patterns and regional averages. Their temporal variations were also analyzed to understand the differences in the seasonal and inter-annual variability and long-term between the meteorological and hydrological drought indices. The data from a high-resolution regional climate modeling were used.

2 Methods

2.1 Study region

The study region was the HRB and the adjacent areas (Fig. 1). The Heihe River origins from the Qilian Mountains in the northern edge of the Tibet Plateau and flows northward to the China-Russian border. The HRB spans between 98°~101°30′E and 38°~42°N. The upper HRB is within the mountains elevated 2300~3200m mainly covered with forests and mountain meadows. The middle HRB is along the Hexi Corridor elevated 1600~2300m mainly covered with piedmont steppe grass, crops, and residence and commercial uses. The lower HRB is in the Alxa High-Plain elevated below 1600m mainly covered with Gobi and desert sands.

Nat. Hazards Earth Syst. Sci. Discuss., https://doi.org/10.5194/nhess-2017-310
Manuscript under review for journal Nat. Hazards Earth Syst. Sci.
Discussion started: 16 January 2018

Natural Hazards and Earth System Sciences
Discussions

Annual precipitation is over 400mm in the upper basin, with the maximum of 800mm at extremely high elevations, about 100~250mm in the middle basin, and below 50mm in many lower basin areas. The annual precipitation in the upper basin has high seasonal variability, and nearly 70% of the total annual rainfall occurs from May to September (Gao et al., 2016). The upper basin generates nearly 70% of the total river runoff, which supplies agricultural irrigation and benefits the social economy development in the middle and lower basin reaches (Yang et al., 2015; Chen et al., 2005). Annual mean temperature is about −4°C in the upper basin, 7°C in the middle basin, and nearly 9°C in the lower basin.

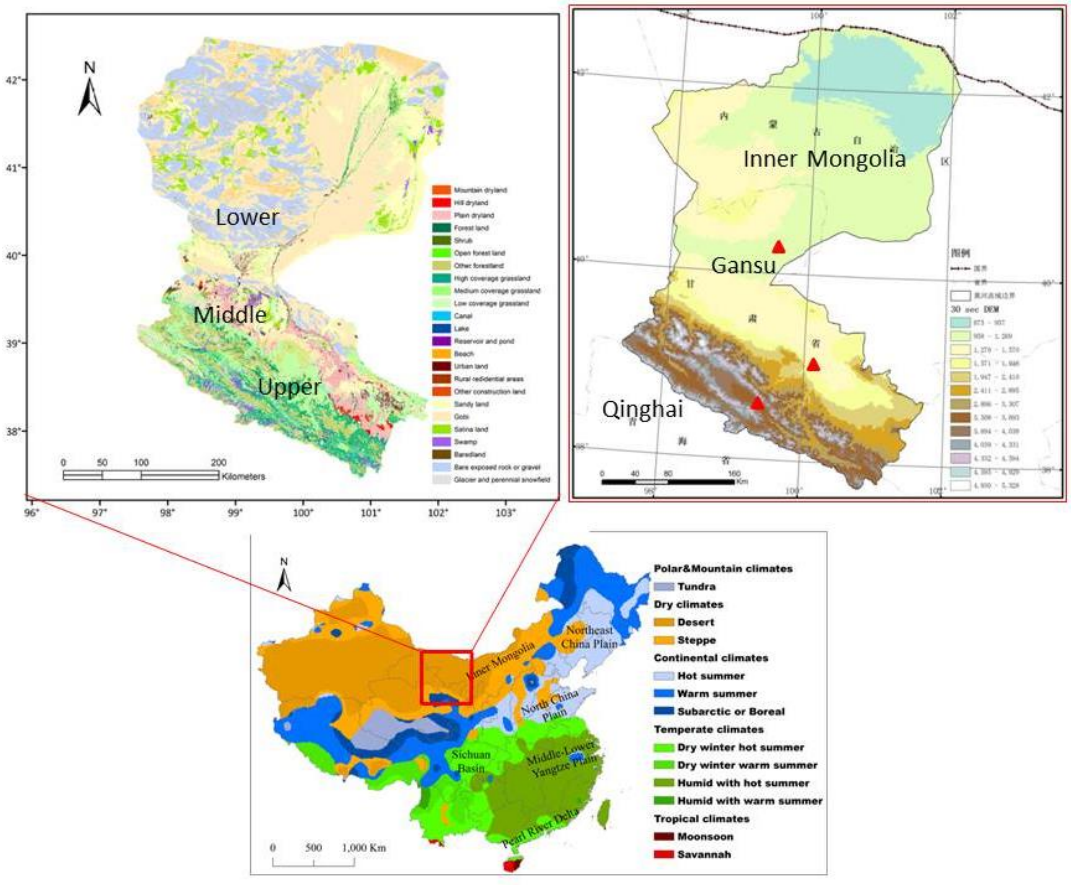

Figure 1. The study region of the Heihe River Basin, with landscape (upper left) and elevation (meter) and three provinces (upper right) (data source: Wang et al., 2014). The triangles signs in upper left are meteorological observation sites. The bottom panel shows the

Nat. Hazards Earth Syst. Sci. Discuss., https://doi.org/10.5194/nhess-2017-310
Manuscript under review for journal Nat. Hazards Earth Syst. Sci.
Discussion started: 16 January 2018

location of the study region in China and the Koppen climate classification (from Peel et al., 2007).

2.2 Drought indices

The meteorological drought index is defined as $AI = P / PET$, where P and PET are daily precipitation and potential evapotranspiration, respectively. AI is a variant of the index originally defined by Budyko (1974), which is the ratio of annual PET to P. The average AI values were used to classify the arid, semi-arid, semi-humid (sub-humid), and humid climate with the ranges of $AI \leq 0.2$, $0.2 < AI \leq 0.5$, $0.5 < AI \leq 1.3$, and $AI > 1.3$, respectively (Ponce et al., 2000).

The hydrological drought index is defined as $ESI = AET / PET$, where AET is daily actual evapotranspiration. The ranges of average ESI values of $ESI \leq 0.1$, $0.1 < ESI \leq 0.3$, $0.3 < ESI \leq 0.6$, and $ESI > 0.6$ were used to classify the arid, semi-arid, semi-humid, and humid climate, respectively (Yang, 2007). This approach agrees with Anderson (2011), which showed that the ESI values varying gradually from 0 to 1 correspond to several USDM drought levels from exceptional to no drought for each month from April to September across the continental U.S.

Two methods were used to estimate PET (mm/d). One was the energy balance based FAO-56 Penman-Monteith Equation (Allen et al. 1998):

$$PET_p = \frac{0.408\Delta(R_n - G) + \gamma \frac{900}{T+273} u_2 (e_s - e)}{\Delta + \gamma(1 + 0.34u_2)} \quad (1)$$

where R_n and G are net radiation and soil flux on the ground ($MJm^{-2}d^{-1}$); T is air temperature (^oC); e_s and e are saturation and actual water vapor pressure (kPa); u_2 is wind speed at 2m above the ground (ms^{-1}); Δ is the rate of change of e_s with respect to T ($kPa/^oC$); γ is the psychrometric constant ($kPa/^oC$). The other method is the temperature based on Hamon formula (Hamon, 1963):

$$PET_h = \frac{k \times 0.165 \times 216.7 \times N \times e_s}{T + 273.3} \quad (2)$$

where k is proportionality coefficient = 1; N is daytime length. e_s is in 100 Pa here.

Monthly PET, precipitation and actual evapotranspiration, obtained based on daily values, were used to calculate the drought indices. It was assumed that daily PET=0 if daily $T<0^oC$. Their monthly PET was not used if PET=0 for more than 10 days in a month. In this case, no

Nat. Hazards Earth Syst. Sci. Discuss., https://doi.org/10.5194/nhess-2017-310
Manuscript under review for journal Nat. Hazards Earth Syst. Sci.
Discussion started: 16 January 2018

drought indices were calculated for the month. It was also assumed that daily ground energy was in balance, so $R_n - G = H + L \times AET$, where H and L are sensible heat flux and potential heat constant.

The data used in calculation and evaluation of the drought indices are listed in Table 1.

Table 1. The data used in calculation and evaluation of the drought indices. H, AET, P, T, and e (RH) are sensible heat flux, actual evapotranspiration, precipitation, temperature, wind speed, and water vapor pressure (relative humidity). HRB stands for Heihe River Basin.

Source	Parameter	Time Period	Space	Reference
Simulation	H, AET, P,T, u, e	1980-2010, daily	HRB, 3 km resolution	Xiong and Yan (2013)
Observation	P,T,RH	1980-2010, daily	3 sites in HRB	China National Met Sci Infrastructure (data.cma.cn)

2.3 Regional climate modeling

The climatic and hydrological data used to calculate the drought indices were created from a regional climate modeling using the Regional Integrated Environmental Model System (RIEMS 2.0) (Xiong and Yan, 2013). The simulation was conducted over the period of 1980-2010. The horizontal spatial resolution was 3km. A unique feature with this simulation was that the model's parameters, including soil hydrological properties, were recalibrated based on observations and remote sensing data over the HRB that greatly improved the model's performance. The model evaluation indicated that the model was able to reproduce the spatial pattern and seasonal cycle of precipitation and surface T. The correlation coefficients between the simulated and observed pentad P were 0.81, 0.51, and 0.7 in the upper, middle, and lower HRB regions, respectively ($p<0.01$).

The historical T and P observations during the simulation period at Yeilangou of the upper basin (38.25°N, 99.35°E, 3300m above the sea level), Zhangye of the middle basin (38.11°N, 100.15°E, 1484m), and Dingqing of the lower basin (40.3°N, 99.52°E, 1177m) (Fig. 1) were used to compare with the simulations.

3 Results

3.1 Simulated climate and hydrology

Nat. Hazards Earth Syst. Sci. Discuss., https://doi.org/10.5194/nhess-2017-310
Manuscript under review for journal Nat. Hazards Earth Syst. Sci.
Discussion started: 16 January 2018

196 The spatial pattern of the simulated annual *T* averaged over the simulation period is featured
197 by the large changes between basin reaches, increasing from about -15°C in the tall
198 mountains of the upper basin to over 10°C in the deserts of the lower basin (Fig. S1). The
199 simulated average annual *P* shows an opposite gradient, decreasing from about 2.5 mm/d in
200 the mountains to less than 0.25 mm/d in the deserts (Fig. S2). The simulated average annual
201 *AET* has a similar pattern to precipitation (Fig. S3). The spatial variability is much larger
202 within the upper basin than the lower basin.
203 An interesting feature is that both *T* and *P* in the middle basin are very close to their
204 corresponding values in the lower basin but much different from those in the upper basin; the
205 *AET* difference between the middle and upper basin reaches however is much small.
206 As expected, the regional *AET* values averaged over the simulation period are higher in
207 summer than in winter (Fig. S4). In the upper basin, for example, *T* increases from about -
208 15°C in winter to 10°C in summer, *P* increased from about 0.25 to 4 mm/d, and *AET* from
209 about 0.25 to 2.5 mm/d. Again, *T* and *P* are close between the middle and lower basin
210 reaches all seasons, and *AET* is close between the middle and upper basin reaches during
211 winter and spring. While *AET* is close between the middle and lower basin reaches during
212 summer and fall, the differences between the middle and upper basin reaches are much
213 smaller than the differences in *T* or *P*.
214 The inter-annual variability of regional *T* and *P* is similar between the middle and lower
215 basin reaches (Fig. S5). A few dry years (e.g., 1990, 2001, and 2008) and wet years (e.g.,
216 1981, 1989, 2002, and 2007) can be found. The amplitude of variability is larger for *P* than *T*,
217 especially in the upper basin. The variability of *AET* is also similar between the lower and
218 middle basin reaches, but it differs from that in the upper basin during some periods (e.g.,
219 around 1985). The differences in *AET* between the middle and upper basins are much smaller
220 in the magnitude than those for the meteorological properties.
221 The above features of close values and similar inter-annual variability in the simulated *T*
222 and *P* between the middle and lower basin reaches are also seen in the observations (Fig. S6).
223 The simulated *T* in all basin regions and *P* in the middle and lower basin reaches are close to
224 the observed ones. However, the simulated *P* is about 0.4 mm/d higher (about 1.6 mm/d for
225 simulation vs. 1.2 mm/d for observation). The weather site in the upper basin is located in

Nat. Hazards Earth Syst. Sci. Discuss., https://doi.org/10.5194/nhess-2017-310
Manuscript under review for journal Nat. Hazards Earth Syst. Sci.
Discussion started: 16 January 2018

relatively flat and low valley, while the simulation grids have many points at high elevations where *P* is larger than at the valley locations.

The simulated *P* increases around 50% over the simulation period, statistically significant at p<0.01in all basin reaches (Table S1). The simulated *AET* also increases, but at a smaller degree of around 20% and p<0.01 only in the upper basin. The simulated *T* shows increasing trends, but insignificant in all reaches. The simulated *P* trends are close to the observed ones in the middle and lower basin reaches, but opposite to that in the upper basin. The simulated *T* underestimates the observed warming, which was about 2^{o}C at p<0.01.

3.2 Spatial patterns of drought indices

PET calculated using the Penman-Monteith method is mostly 1.7-2.25 mm/d in the upper basin (Fig. 2). It increases to above 3 mm/d in the middle and lower basins. There is little difference between the two regions. The meteorological drought index, *AI*, shows a similar pattern but opposite gradient (Fig. 3). It is as large as 1.4 in the upper basin, but reduced to less than 0.2 in two other basin regions, indicating increasing aridity from the upper to lower basin. The hydrological drought index, *ESI*, has the same gradient as *AI*, but with different spatial pattern (Fig. 4). It is as high as 0.9 in the upper basin and reduced to mostly below 0.1 in the lower basin. However, the values in the middle basin is as high as 0.6, much larger than that in the lower basin.

P and *AET* are the highest in the upper basin and the lowest in the lower basin, while *T* and *PET* have an opposite seasonal cycle. This explains why *AI* and *ESI* are larger in the upper basin than the middle or lower basin.

Nat. Hazards Earth Syst. Sci. Discuss., https://doi.org/10.5194/nhess-2017-310
Manuscript under review for journal Nat. Hazards Earth Syst. Sci.
Discussion started: 16 January 2018

Natural Hazards and Earth System Sciences
Discussions

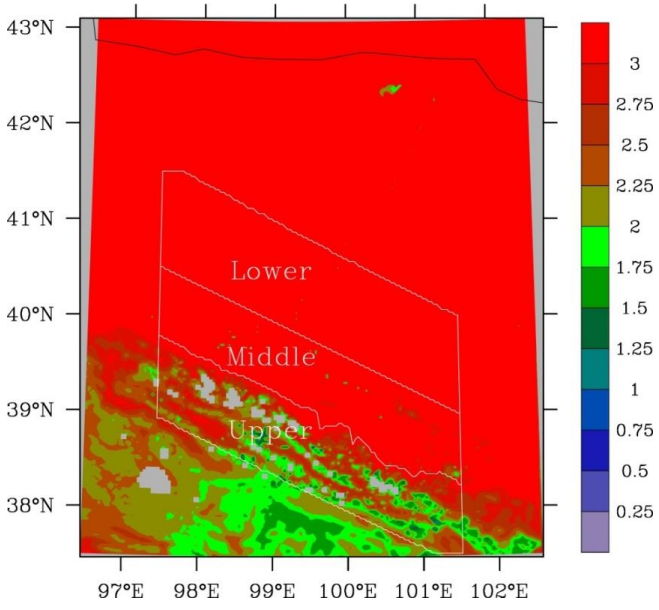

Figure 2. Spatial distributions of potential evapotranspiration (*PET*, mm/d) estimated using the Penman-Monteith method.

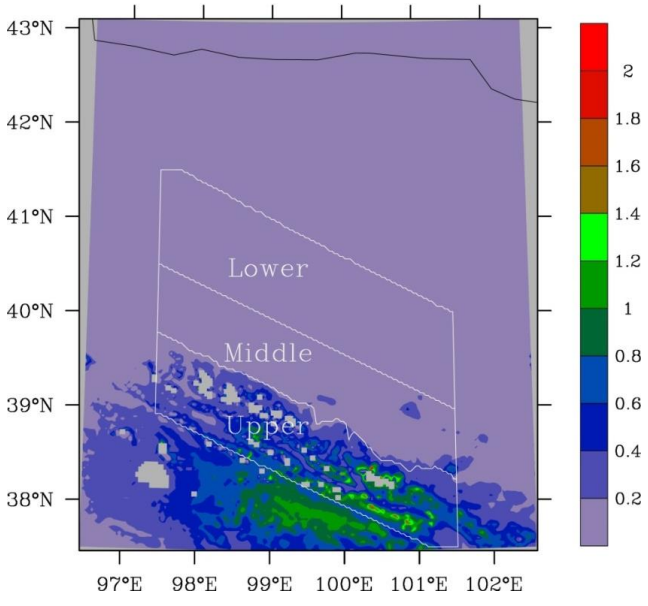

Figure 3. Spatial distributions of aridity index with potential evapotranspiration estimated using the Penman-Monteith method.

Nat. Hazards Earth Syst. Sci. Discuss., https://doi.org/10.5194/nhess-2017-310
Manuscript under review for journal Nat. Hazards Earth Syst. Sci.
Discussion started: 16 January 2018

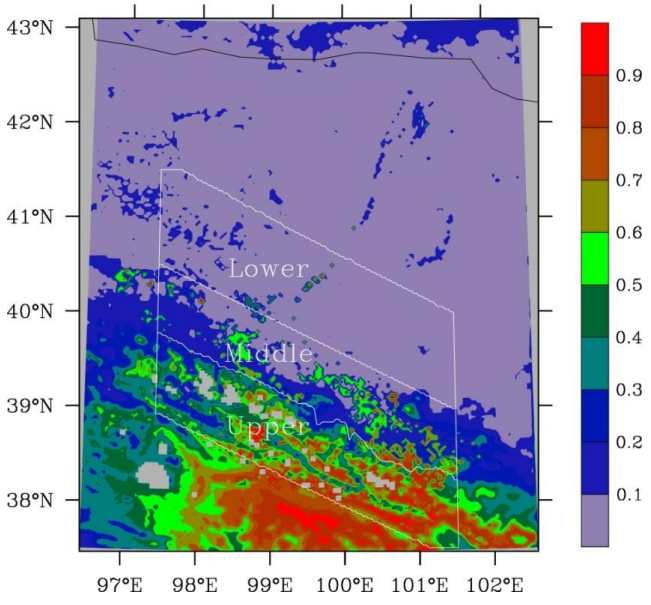

Figure 4. Spatial distributions of evaporative stress index with potential evapotranspiration estimated using the Penman-Monteith method.

PET calculated using the Hamon method has the same pattern as the one using the Penman-Monteith method, but with smaller magnitude (Fig. 5). *PET* is mostly about 1 mm/d in the upper basin and increases to about 1.5-1.75 mm/d in the middle basin, and further to 1.75-2.25 mm/d in the lower basin.

The different spatial patterns between *AI* and *ESI* seen above are also found for the Homan method. *AI* is mostly above 0.6 in the upper basin (Fig. 6). It is below 0.2 in the middle and lower basins without apparent differences between the two regions. In contrast, while *ESI* remains large values of mostly above 0.9 in the upper basin and low values of below 0.2 in the lower basin, the values in many areas of the middle basin are 0.4-0.9, much different from those in the lower basin (Fig. 7).

Nat. Hazards Earth Syst. Sci. Discuss., https://doi.org/10.5194/nhess-2017-310
Manuscript under review for journal Nat. Hazards Earth Syst. Sci.
Discussion started: 16 January 2018

Natural Hazards and Earth System Sciences
Discussions

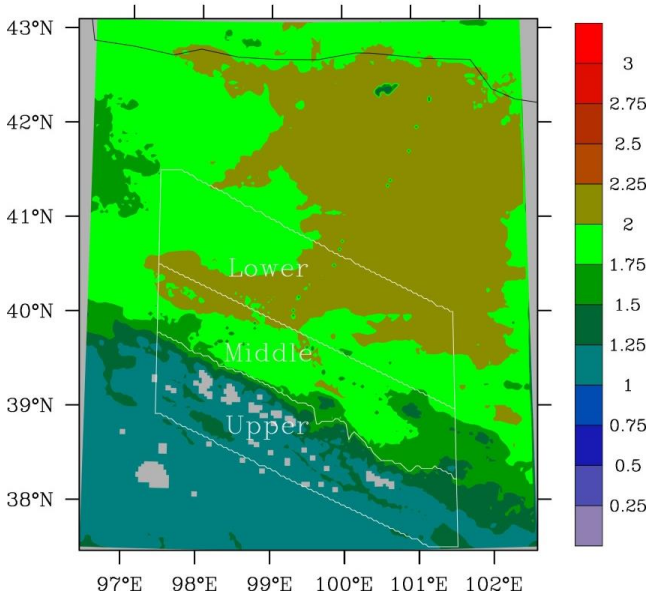

Figure 5. Spatial distributions of potential evapotranspiration (*PET*, mm/d) estimated using the Hamon method.

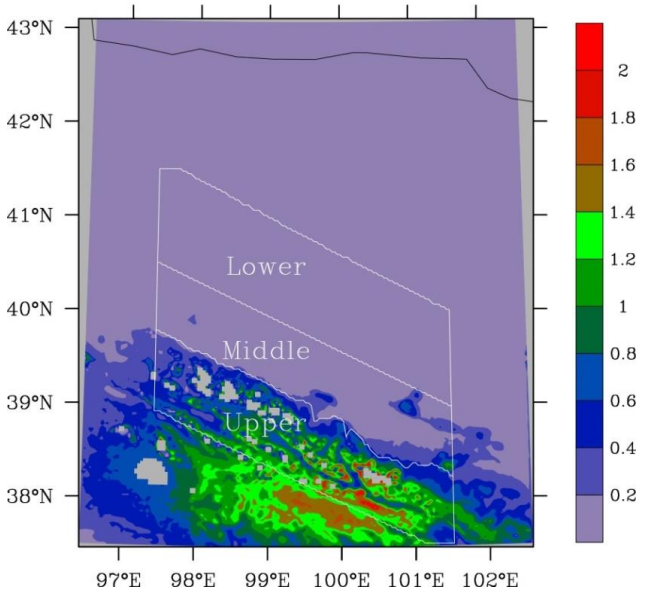

Figure 6. Spatial distributions of aridity index with potential evapotranspiration estimated using the Hamon method.

Nat. Hazards Earth Syst. Sci. Discuss., https://doi.org/10.5194/nhess-2017-310
Manuscript under review for journal Nat. Hazards Earth Syst. Sci.
Discussion started: 16 January 2018

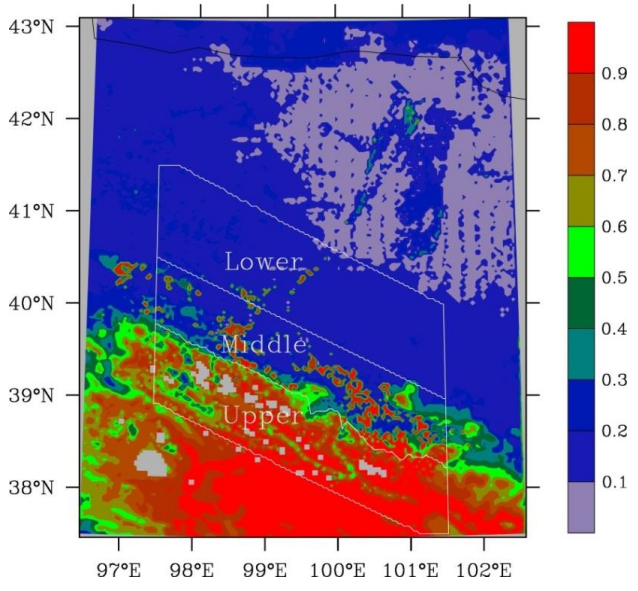

Figure 7. Spatial distributions of evaporative stress index with potential evapotranspiration estimated using the Hamon method.

3.3 Climate classification

The annual *PET* averages over 1980-2010 calculated using the Penman method are 2.12, 3.91, and 4.76 (Table 2 and Fig. 8). The corresponding *AI* values are about 0.9, 0.12, and 0.04, falling into semi-humid, arid, and arid climate. The corresponding *ESI* values are 0.63, 0.22, and 0.07, falling into humid, semi-arid, and arid climate. The annual *PET* averaged over 1980-2010 calculated using the Homan method are 1.25, 2.33, and 2.65 mm/d for the upper, middle, and lower basin reaches. The corresponding *AI* values are about 1.3, 0.18, and 0.07, falling into humid, arid, and arid climate. The corresponding *ESI* values are 0.78, 0.31, and 0.13, falling into humid, semi-humid, and semi-arid climate.

Thus, the climate across the HRB classified using *AI* has two types of semi-humid (the Penman method for *PET*) or humid (the Homan method) in the upper basin, and arid in both middle and lower basin reaches. In contrast, the climate classified using *ESI* has three types of humid in the upper basin, semi-arid (the Penman method) or semi-humid (the Homan method) in the middle basin, and arid (the Penman method) or semi-arid (the Homan method)

Nat. Hazards Earth Syst. Sci. Discuss., https://doi.org/10.5194/nhess-2017-310
Manuscript under review for journal Nat. Hazards Earth Syst. Sci.
Discussion started: 16 January 2018

295 in the lower basin. This indicates that only the hydrological drought index is able to identify
296 the transition climate zone in the middle basin.

297 The difference between *AI* and *ESI* in classifying climate is related to the similar feature
298 with the meteorological variables. Annual *P* is 555 mm in the upper basin, which is
299 substantially different from 69-139 mm in the middle and lower basins. The mean *T* is -4.0°C
300 in the upper basin, which is well below 6.9-8.7°C in the middle and lower basin reaches. The
301 corresponding *PET* values fall into two groups, 299 mm in the upper basin and 672-767 mm
302 in the middle and lower basin reaches. This explains why the *AI* falls into two groups. In
303 contrast, *AET* is 226, 161, and 80 mm, substantially different not only between the middle
304 and upper reaches but also between the middle and lower reaches. This explains why the *ESI*
305 falls into three groups.
306
307 Table 2. Regional average (AVE), standard deviation (SD), and coefficient of variation (CV)
308 for potential evapotranspiration (*PET*, mm/d), aridity index (*AI*), and evaporative stress index
309 (*ESI*).

PET	Basin	PET			AI			ESI		
		AVE	SD	CV	AVE	SD	CV	AVE	SD	CV
Penman-Monteith	Upper	2.12	0.12	0.06	0.90	0.32	0.35	0.62	0.07	0.11
	Middle	3.91	0.21	0.05	0.12	0.06	0.50	0.22	0.06	0.26
	Lower	4.76	0.29	0.06	0.04	0.03	0.64	0.07	0.03	0.41
Hamon	Upper	1.25	0.04	0.03	1.30	0.37	0.29	0.78	0.05	0.07
	Middle	2.33	0.11	0.05	0.18	0.08	0.43	0.31	0.06	0.19
	Lower	2.65	0.16	0.06	0.07	0.04	0.56	0.13	0.04	0.31

310

311 **3.4 Temporal variations of drought indices**

312 **3.4.1 Seasonal cycle**

313 For the Penman-Monteith method, *PET* is the highest in summer and smallest in winter (Fig.
314 8). Note that winter PET in the upper basin is not shown because *T* is below zero in too many
315 days. The amplitude in the middle basin is close to that in the lower basin, but much larger
316 than that in the upper basin. Different from the upper basin where *AI* and *ESI* are also the
317 largest in summer, *AI* is the largest in fall, while *ESI* is the largest in winter in the middle
318 basin (as well as lower basin). The seasonal variations of *PET*, *AI* and *ESI* estimated using
319 the Homan method are similar to those using the Penman method.

Nat. Hazards Earth Syst. Sci. Discuss., https://doi.org/10.5194/nhess-2017-310
Manuscript under review for journal Nat. Hazards Earth Syst. Sci.
Discussion started: 16 January 2018

320 The seasonal AI and ESI cycles are related to those of the meteorological and
321 hydrological conditions. *T*, *P* and *AET* (Fig. S4), and *PET* (Fig. 8) all increase from winter to
322 summer. In the upper basin, the increases in *P* and *AET* from spring / fall to summer are
323 larger than the corresponding increases in *PET*, leading to larger *AI* and *ESI* values in
324 summer. In the middle as well as lower basin, however, *PET* increases substantially from
325 spring / fall, leading to smaller *AI* and *ESI* in summer than in spring / fall.
326

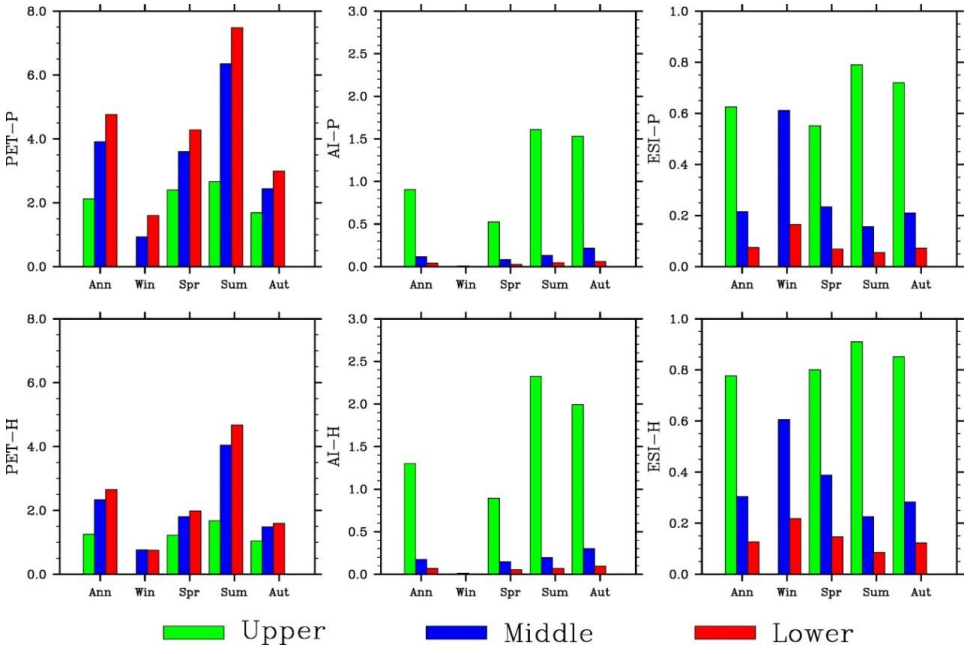

327
328 Figure 8. Seasonal variations of simulated potential evapotranspiration (*PET*, mm/d), aridity
329 index (*AI*), and evaporative stress index (*ESI*) (from left to right). The top and bottom panels
330 are for the Penman-Monteith and Hamon method, respectively.
331
332 **3.4.2 Inter-annual variability**
333 *PET* in the middle basin calculated using the Penman-Monteith method shows similar inter-
334 annual variability over the period of 1980-2010 to that in the lower basin, but much different
335 from that in the upper basin (Fig. 9). The standard deviation (SD) increases from the upper
336 (0.12) to middle (0.21) and to lower basin (0.29) (Table 2). The coefficient of variation (CV)

Nat. Hazards Earth Syst. Sci. Discuss., https://doi.org/10.5194/nhess-2017-310
Manuscript under review for journal Nat. Hazards Earth Syst. Sci.
Discussion started: 16 January 2018

Natural Hazards and Earth System Sciences
Discussions

337 (the ratio of the standard deviation to the average), a statistical property often used to
338 measure relative variability intensity, however, is comparative among the reaches.
339

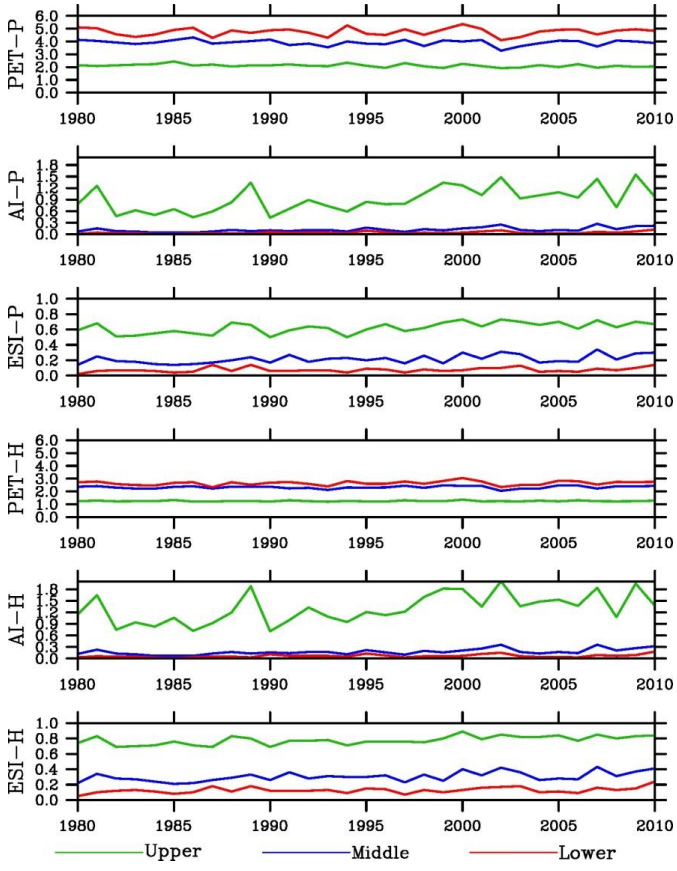

340
341 Figure 9. Inter-annual variations of potential evapotranspiration (*PET*, mm/d), aridity index
342 (*AI*), and evaporative stress index (*ESI*). P and H indicates the Penman-Monteith and Hamon
343 method, respectively.
344
345 The SD values of both *AI* and *ESI* decrease from the upper to middle and to lower basin.
346 However, SD of *AI* (*ESI*) in the middle basin is much closer to that in the lower (upper) basin.
347 The CV values have opposite gradient to SD, increasing from the upper to middle and to
348 lower basin. In addition, CV differs mainly not between the basin reaches but between
349 drought indices: *AI* is larger than *ESI*.

Nat. Hazards Earth Syst. Sci. Discuss., https://doi.org/10.5194/nhess-2017-310
Manuscript under review for journal Nat. Hazards Earth Syst. Sci.
Discussion started: 16 January 2018

350

351 **3.4.3 Long-term trends**

352 *PET* shows little trends over the simulation period (Table 3). On contrast, drought indices
353 increased dramatically, by 60% or more for *AI* and 15-50% for *ESI*. The trends are
354 significant at $p<0.01$ in the upper and middle basin reaches and $p<0.05$ in the lower basin.
355 Table 3. Mann-Kendall trends from 1980 to 2010 of potential evapotranspiration (*PET*,
356 mm/d), aridity index (*AI*), and evaporative stress index (*ESI*). P (H) indicates the Penman-
357 Monteith (Hamon) method. The bold and italic numbers are significant at $p<0.01$ and $p<0.05$,
358 respectively.
359

Index	Upper	Middle	Lower
PET-P	*-7.3*	-2.7	0.3
AI-P	**72.5**	**98.6**	*80.9*
ESI-P	**24.8**	**51.4**	*47.8*
PET-H	0.0	2.7	3.6
AI-H	**62.6**	**84.3**	*66.3*
ESI-H	**16.2**	**40.8**	*40.5*

360

361 **3.5 Extreme events**

362 The drought indices for 4 simulated dry years (1982, 1990, 2001, and 2008) and 4 wet years
363 (1981, 1989, 2002, and 2007) (Figs.S7-8) and the averages over the dry or wet years (Fig. 10)
364 were analyzed. The annual *AI* values using the Penman-Monteith method are 0.4-0.5 for the
365 first two dry years and 0.7-1.0 for the last two years in the upper valley (Fig. 10). The
366 average over the 4 years is about 0.65. In comparison, the average is about 0.9 over 1980-
367 2010 and 1.4 over the 4 wet years. The values are very small in spring (except in 1982) and
368 occasionally in fall (1990). The annual *AI* values in the middle and lower basin reaches are
369 below 0.2 for individual dry years and average. The small values are found for individual
370 seasons except falls of the last two years in the middle basin. In compassion, the annual
371 values are 0.4 or above in 3 falls of the 4 wet years.

372 The annual *ESI* values using the Penman-Monteith method are 0.5 or larger in the upper
373 valley. The average over the 4 years are nearly 0.6. In comparison, the average is about 0.62
374 over 1980-2010 and 0.7 over the 4 wet years. The values are comparable from spring to fall,
375 though relatively smaller in spring. This is different from AI. The annual *ESI* values are

Nat. Hazards Earth Syst. Sci. Discuss., https://doi.org/10.5194/nhess-2017-310
Manuscript under review for journal Nat. Hazards Earth Syst. Sci.
Discussion started: 16 January 2018

Natural Hazards and Earth System Sciences
Discussions

about 0.2 in the middle and below 0.1 in the lower basin for individual dry years and average. Thus, the values are apparently different between the middle and lower basin reaches. This is another difference from AI. The lowest values mostly occur in summer in both basin reaches. In compassion, the annual values are 0.25-0.35 in the middle basin and 0.1 or larger in 3 of the 4 wet years in the lower basin.

Same results, that is, substantially smaller *AI* than normal, especially in spring but no much *ESI* changes from normal and between seasons in the upper basin, and no much *AI* change from normal and wet events (small in all cases) in the middle and lower basin reaches but much smaller *ESI* than wet events and different between the two basin reaches, can be found for the Hamon method, though slightly larger *AI* and *ESI* values. The results suggest that *ESI* is better representative of extreme dry conditions in the middle basin, but less sensitive to drought in the upper basin.

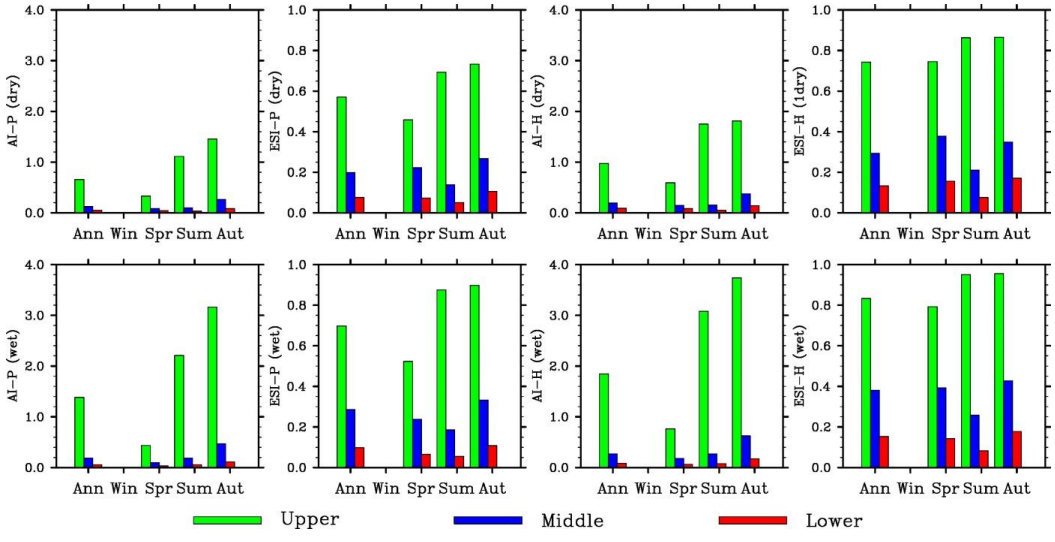

Figure 10. Seasonal variations of simulated aridity index (*AI*), and evaporative stress index (*ESI*) using the Penman-Monteith and Hamon methods (left to right) for averages over the dry years of 1982, 1990, 2001, 2008 (top) and (bottom).

4 Discussion

4.1 Importance of land-surface processes

The HRB is a typical inland river basin with a strong contrast in topography, landscape, climate, and human activities from the headwater to end point along its drainage system. The water shortage and frequent droughts are the biggest environmental threat to the ecosystems and human activities in this region as well as entire northwestern China. The HRB is well studied for understanding the interactions among eco-hydrological and socio-economical processes. This comparison study provides evidence for the importance of water and energy interactions between land process and the atmosphere and between upstreams and downstreams in determining climate types in an arid climate.

Because the *ESI* values are related to *AET* that is controlled by land-surface properties and management practices (e.g., rainfall-fed crops vs irrigated crops; natural wetlands vs cultivated drained croplands), our results suggest the land-surface processes play an important role in affecting drought conditions and their variability. The landscape in the HRB, especially its transition zone, has changed remarkably in the past several decades due to urbanization, farming, and grazing activities (Hu et al., 2015). The irrigation may have caused the lower basin more water stressed (higher *ESI* than *AI*) since stream water from Heihe is intercepted and rivers go dry downstreams. The *ESI* should reflect this change since it is calculated partially based on the land-surface hydrological conditions. The regional land-atmosphere coupled models would provide proofs for this hypothesis though modeling the impacts of land cover change, which is a driver of local land-atmosphere interactions.

4.2 Role in moderating climate

The magnitude of *AI* (*ESI*) inter-annual variability in the middle basin is (in not) very close to that in the lower basin, another evidence for the unique capacity of *ESI* in separating the climate zones between the middle and lower basin reaches. The magnitude of the relative inter-annual variability differs mainly between *AI* and *ESI*, larger with *AI*. In addition, both *AI* and *ESI* in the HRB decreased dramatically from 1980 to 2010, at greater rate with *AI*. Thus, the drought conditions described using *ESI* is less variable, suggesting the role of local hydrological processes in moderating extreme climate events.

4.3 Future trends

One of the hydrological consequences from the projected climate change due to the greenhouse gas increase is more frequent and intense droughts in watersheds of dry regions. In the Colorado River Basin, global warming may lead to substantial water supply shortages (McCabe and Wolock, 2007), and the climate models projected considerably more drought activities in the 21st century (Cayan et al., 2010). In the HRB, the climate of the upper HRB will likely become warmer and wetter in the near future (Zhang et al., 2016), consistent with the historical records. Correspondingly the basin-wide evapotranspiration, snowmelt, and runoff are projected to increase over the same period. Many drought indices, including the *AI*, have been used to project future drought trends (Paulo et al., 2012). However, most of the recent ESI studies are based on historical remote sensing for monitoring short-term drought development, which limits the application of this drought index to climate change and drought impact research. Due to the unique ability with the *ESI* in identifying the transition climate zone as shown in this study, it would be valuable to explore its potential for future drought projection study and compare with that of the *AI*.

4.4 Uncertainty and future research

The regional climate simulation which generated data for this analysis has many uncertainties (Xiong and Yan, 2013). One of the contributing factors is the very limited number of meteorological, hydrological, and ecological measurement sites. A large-scale, multiple-year field experiment project has been conducted in the HRB, which have been generating extensive datasets (Wang et al., 2014). These data are being used to improve the regional climate modeling, which will in turn generate new high-resolution data for further drought analysis. Furthermore, the regional climate modeling has been expanded into the middle 21st century, providing data for calculating the drought indices and comparing their future trends. Comparisons of other meteorological and hydrological drought indices are also a future research issue.

5 Conclusions

This study has found that the *ESI* climate classification agrees with the Koppen climate classification (Peel et al., 2007). By this system, we found that the climate types are different among the upper, middle, and lower HRB. In contrast, there would be no difference between

457 the middle and lower HRB regions when the *AI* was used. The comparison results from this
458 study therefore suggest that only ESI is able to identify a transition climate zone between the
459 relatively humid climate in the mountains and the arid climate in the Gobi desert region. We
460 conclude that the hydrological drought index *ESI* is a better index than the meteorological
461 drought index *AI* for aridity classification in the HRB with a complex topography and land
462 cover. Selection of the most appropriate drought index facilitates drought characterization,
463 drought assessment and risk mitigation, and water resources management in the arid region.
464
465 **Acknowledgement** This study was supported by the National Natural Science Foundation of
466 China (NSFC) (No. 91425301) and the USDA Forest Service.
467
468 **References**
469 Allen, R. G., Pereira, L. S., Raes, D., and Smith, M.: "Crop evapotranspiration: guidelines for
470 computing crop water requirements." Irrigation and Drainage Paper No. 56, Food and
471 Agriculture Organization of the United Nations, Rome, Italy, 1998.
472 Anderson, M. C., Hain, C. R., Wardlow, B., Mecikalski, J. R., and Kustas, W. P.: Evaluation
473 of drought indices based on thermal remote sensing of evapotranspiration over the
474 continental U.S. Journal of Climate, 24, 2025–2044, 2011.
475 Anderson, M. C., Zolin, C. A., Sentelhas, P. C., Hain, C. R., Semmens, K., Yilmaz, M. T.,
476 Gao, F., Otkin, J. A., and Tetrault, R.: The Evaporative Stress Index as an indicator of
477 agricultural drought in Brazil: An assessment based on crop yield impacts, Remote
478 Sensing of Environment, 174, 82–99, doi:10.1016/j.rse.2015.11.034, 2016.
479 Arora, V. K.: The use of the aridity index to assess climate change effect on annual runoff，
480 Journal of Hydrology, 265, 164-177, 2002.
481 Budyko, M. I.: Climate and Life, Academic, San Diego, CA, 508 pp., 1974.
482 Cayan, D. R., Das, T., Pierce, D. W., Barnett, T. P., Tyree, M., and Gershunov, A.: Future
483 dryness in the southwest US and the hydrology of the early 21st century drought, Proc.
484 Natl. Acad. Sci., 107, 21, 271–21, 276. http://research001.com/?showinfo-140-577279-
485 0.html, 2010.

Chen, Y., Zhang, D., Sun, Y., Liu, X., Wang, N., and Savenije, H.: Water demand management: A case study of the Heihe River Basin in China. Phys. Chem. Earth, 30, 408–419, http://dx.doi.org/10.1016/j.pce.2005.06.019, 2005.

Choi, M., Jacobs, J. M., Anderson, M. C., and Bosch, D. D.: Evaluation of drought indices via remotely sensed data with hydrological variables, Journal of Hydrology, 476, 265-273. doi:10.1016/j.jhydrol.2012.10.042, 2013.

Gao, B., Qin, Y., Wang, Y. H., Yang, D., and Zheng, Y.: Modeling Ecohydrological Processes and Spatial Patterns in the Upper Heihe Basin in China, Forests, 7(1). doi:10.3390/f7010010, 2016.

Hamon, W. R.: Computation of direct runoff amounts from storm rainfall. Intl. Assoc. Scientific Hydrol. Publ., 63, 52- 62, 1963.

Hu, X., Lu, L., Li, X., Wang, J., and Guo, M.: Land use/cover change in the middle reaches of the Heihe River Basin over 2000-2011 and its implications for sustainable water resource management. PLoS ONE 10(6): e0128960. doi:10.1371/journal.pone.0128960, 2015.

Li, J.: Multivariate Frequencies and Spatial Analysis of Drought Events Based on Archimedean Copulas Functio, Northwest University of Science and Technology, 2012.

McCabe, G. J., and Wolock, D. M.: Warming may create substantial water supply shortages in the Colorado River basin, Geophysical Research Letters, 34, 22, 2007.

Onder, D., Aydin M., Berberoglu, S., Onder, S., and Yano, T.: The use of aridity index to assess implications of climatic change for land cover in Turkey. Turkish Journal of Agriculture and Forestry, 33, 305-314, 2009.

Otkin, J. A., Anderson, M. C., Hain, C. R., Mladenova, I. E., Basara, J. B., and Svoboda, M.: Examining rapid onset drought development using the thermal infrared based Evaporative Stress Index, Journal of Hydrometeorology, 14, 1057–1074, 2013.

Paulo, A. A., Rosa, R. D., and Pereira, L. S.: Climate trends and behavior of drought indices based on precipitation and evapotranspiration in Portugal, Nat. Hazards Earth Syst. Sci., 12, 1481–1491, 2012.

Peel, M. C., Finlayson, B. L., and McMahon, T. A.: Updated world map of the Köppen–Geiger climate classification. Hydrol. Earth Syst. Sci., 11, 1633–1644. doi:10.5194/hess-11-1633-2007, 2007.

Ponce, V. M., Pandey, R. P., and Ercan, S.: Characterization of drought across climatic spectrum. Journal of Hydrologic Engineering, ASCE 5, 222–2245, 2000.

Ren, Z., Lu, Y., and Yang, D.: Drought and flood disasters and rebuilding of precipitation sequence in Heihe River basin in the past 2000 years, J. Arid Land Resour. Environ., 24, 91–95, 2010.

Svoboda, M., LeComte, D., Hayes, M., Heim, R., Gleason, K., Angel, J., Rippey, B., Tinker, R., Palecki, M., Stooksbury, D., Miskus, D., and Stephin, S.: The Drought Monitor, Bulletin of the American Meteorological Society, 83, 1181-90, 2002.

UNESCO, Map of the World Distribution of Arid Regions. MAB Techn. Note 7, 1979.

Wolfe, S. A.: Impact of increased aridity on sand dune activity in the Canadian Prairies. Journal of Arid Environments, 36, 421-432, 1997.

Wang, L. X., Wang, S. G., and Ran, Y. H.: Data sharing and data set application of watershed allied telemetry experimental research, IEEE Geoscience and Remote Sensing Letters, 11, 2020-2024, 10.1109/LGRS.2014.2319301, 2014.

Woodhouse, C. A., Meko, D. M., MacDonald, G. M., Stahle, D. W., and Cook, E. R.: A 1,200-year perspective of 21st century drought in southwestern North America. Proc. Natl. Acad. Sci. USA, 107, 21283–21288, 2010.

Xiong, Z., and Yan, X. D.: Building a high-resolution regional climate model for the Heihe River Basin and simulating precipitation over this region. Chin. Sci. Bull, 58, 4670-4678, doi: 10.1007/s11434-013-5971-3, 2013.

Yang, D. W., Gao, B., Jiao, Y., Lei, H. M., Zhang, Y. L., Yang, H. B., and Cong, Z. T.: A distributed scheme developed for eco-hydrological modeling in the upper Heihe River. Sci. China Earth Sci., 58, 36–45. http://dx.doi.org/10.1007/s11430-014-5029-7, 2015.

Yang, G. H.: Agricultural Resources and Classification, China Agricultural Press, Beijing, China, 286 pp., 2007.

Yao, A. Y. M.: Agricultural potential estimated from the ratio of actual to potential evapotranspiration, Agricultural Meteorology, 13, 405-417, doi: 10.1016/0002-1571(74)90081-8, 1974.

Zhang, A. J., Liu, W. B., Yin, Z. L., Fu, G. B., and Zheng, C. M.: How will climate change affect the water availability in the Heihe River Basin, Northwest China? J. Hydrometeorology, doi: http://dx.doi.org/10.1175/JHM-D-15-0058.1, 2016.